THE TOTAL CROSS-SECTION AT THE LHC*

P.V. Landshoff

Centre for Mathematical Sciences
Cambridge CB3 0WA, UK
PVL@damtp.cam.ac.uk

(Received May 12, 2008)

We do not have the ability to perform precise calculations of long-range strong interaction effects, because the effective QCD coupling is not small and so we cannot use perturbation theory. Nevertheless, I will show that we know a lot, though not nearly enough. As a measure of our lack of knowledge, the best prediction for the total cross-section at LHC energy is: $\sigma^{\rm LHC} = 125 \pm 25$ mb.

PACS numbers: 12.40.Nn, 13.85.–t, 13.60.–r

1. Regge theory

This article is about the long-range strong interaction at high energy. Much of what I know about this subject comes from my long collaboration with Sandy Donnachie. A few years ago together with colleagues from the Heidelberg University we wrote a book about it [1]. Most of the material in this paper is taken from the book, and references to papers and data may be found in it.

Because we do not have the ability to perform precise calculations of long-range strong interaction effects, much of what we know comes from looking at experimental data, and so this paper contains rather more data plots than equations. In order to use what understanding we have of the theory and apply it to the data, we have to introduce extra assumptions. I will show that, often, making the simplest possible assumptions turns out to be very successful.

The basic theory is known as Regge theory. It relates together a large number of different reactions. Among those that I will discuss are:

- hadron–hadron total cross-section,
- hadron–hadron elastic scattering,

* Presented at the School on QCD, Low-x Physics, Saturation and Diffraction, Copanello, Calabria, Italy, July 1–14, 2007.

- diffraction dissociation,
- photon and lepton induced reactions.

I will show that we know a lot, but of course not nearly enough. As a measure of our lack of knowledge, the best prediction for the total cross-section at LHC energy is:

$$\sigma^{\mathrm{LHC}} = 125 \pm 25 \text{ mb}\,.$$

By this I mean that 15 years ago I would have predicted 100 mb with some confidence, and it is still quite likely that this will prove to be correct. But a value as large as 150 mb is also quite possible.

Let us have a short glance at the history of strong interactions that finally led to Regge theory:

- 1935: Yukawa predicted the existence of the pion — its exchange generates the static strong interaction,

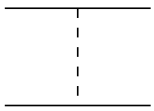

Fig. 1. Graphical representation of one pion exchange.

- 1960s: Nearly everybody worked on the applications of Regge theory, which sums the exchanges of many particles and generates the high-energy strong interaction.
- The known particles not are enough — we need to include exchange of another object, the Pomeron.
- 1970s: QCD is discovered — the BFKL equation generates Pomeron exchange as gluon exchange, but it makes total cross-section rise with energy much faster than is observed.
- Early 1990s: HERA finds a sharp rise of $F_2(x, Q^2)$ at small x, apparently described by BFKL Pomeron exchange.
- So there are two Pomerons: soft (nonperturbative) and hard (perturbative).
- Late 1990s: Higher-order perturbative corrections to BFKL exchange spoil the calculation — this problem is not yet solved, and we do not know whether the hard Pomeron is related to the BFKL equation.

The mathematics to study Pomeron exchange is sophisticated and similar to that used to study diffraction in optics, and it leads to elastic scattering differential cross-section reminiscent of optical diffraction (see Fig. 2):

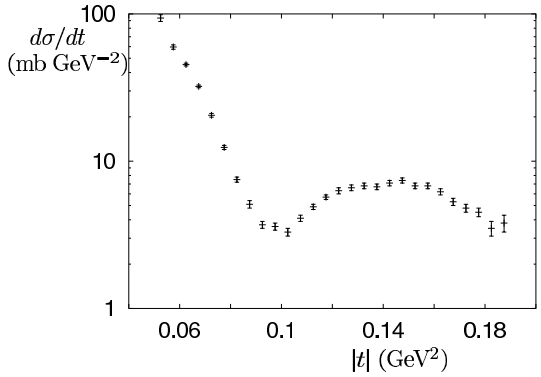

Fig. 2. Elastic $\alpha\alpha$ scattering at 126 GeV CM energy.

But "diffractive" processes in particle physics are more complicated than in optics.

The main ingredient of Regge theory is a concept of Regge trajectory. Regge trajectory describes a set of physical particles whose spins (J) are proportional to their squared masses ($m^2 = t$). In Fig. 3 we show 4 degenerate families of particles: $J = \alpha(t) \approx \frac{1}{2} + 0.9\ t$. The particles in square brackets are listed in the data tables, but there is some uncertainty about whether they exist. The function $\alpha(t)$ is called a Regge trajectory.

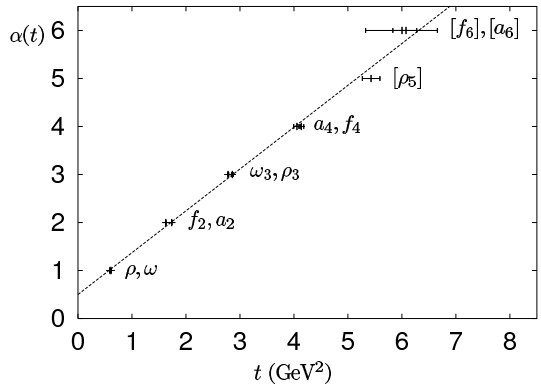

Fig. 3. Plot of spins of families of particles against their squared masses.

Regge theory sums the exchanges of many particles, this is schematically depicted in Fig. 4.

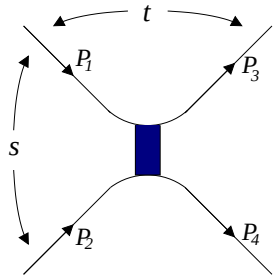

Fig. 4. Kinematics of Regge exchange.

Define

$$\begin{aligned} s &= (P_1+P_2)^2 \quad = \text{squared CM energy}\,, \\ t &= (P_3-P_1)^2 \quad = \text{squared momentum transfer}\,. \end{aligned}$$

At large s but $|t| \ll s$ each trajectory $\alpha_i^{\pm}(t)$ contributes to the amplitude

$$A^{\pm}(s,t) \sim \sum_i \beta_i^{\pm}(t) \Gamma\left(-\alpha_i^{\pm}(t)\right) \left(1 \pm e^{-i\pi\alpha_i^{\pm}(t)}\right) \left(\frac{s}{s_0}\right)^{\alpha_i^{\pm}(t)-1} \qquad (1)$$

with $\pm$ according to the C-parity of the exchange. We know nothing about the function $\beta_i^{\pm}(t)$, except that it is real. $\Gamma(-\alpha_i^{\pm}(t))$ has a pole when $\alpha_i^{\pm}(t)$ is a negative integer, but the signature factor $(1 \pm e^{-i\pi\alpha_i^{\pm}(t)})$ vanishes when $\alpha_i^{\pm}(t)$ is odd/even. The signature factor is the only factor that is not real.

The mathematical formalism that is used to derive this high-energy behaviour of a scattering amplitude was developed by Watson and Sommerfeld in the middle of the 19th century. It starts with the partial-wave series for the amplitude, which is a sum over orbital angular momentum values $\ell = 0, 1, 2, \ldots$. This sum is converted into an integral over ℓ, which becomes a continuous complex variable. So the partial-wave amplitude $a_\ell(s)$ becomes a function $a(\ell, s)$ and it has singularities in the complex-ℓ plane. It turns out that a trajectory $\alpha(t)$ corresponds to a simple pole at $\ell = \alpha(t)$. As I have indicated, a Regge pole at this point in the complex-ℓ plane contributes a power $s^{\alpha(t)-1}$ to the high-energy behaviour of the physical amplitude.

Unfortunately, we know that simple poles are not the only singularities of $a_\ell(s)$. It also has branch points, and we do not know enough about these additional singularities to use them to make well-defined calculations. It is this difficulty that brought to a halt the intense activity in Regge theory in the 1960s, and it has still not been solved. I will discuss it in Section 8.

2. Total cross-section: Fits and theoretical bounds

Optical theorem relates amplitude (1) to the total cross-section:

$$\sigma^{\mathrm{TOT}}(s) = \mathrm{Im}\ A(s, t = 0)\,. \tag{2}$$

So each trajectory contributes a fixed power

$$s^{\alpha(0)-1} \sim s^{-\frac{1}{2}} \quad \text{for} \quad \rho, \omega, f_2, a_2 \quad \text{trajectories}\,.$$

Experiment finds that total cross-sections rise gently at large s. So if this is caused by a Regge pole we need another trajectory with $\alpha(0)$ a little > 1. We call this the soft Pomeron trajectory. Probably it corresponds to the exchange of glueballs, though we cannot be sure because the experimental study of the glueball spectrum is so very difficult.

Fits to total cross-section using Eqs. (1), (2) are presented in Fig. 5.

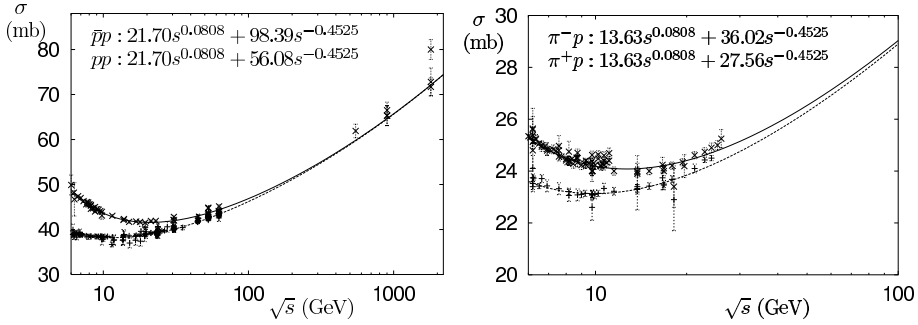

Fig. 5. Fits to total cross-sections for pp, $\overline{p}p$ and $\pi^{\pm}p$ scattering.

A few remarks are here in order:

- We need a Pomeron trajectory with $\alpha_{I\!P}(0) \approx 1.08$. It couples equally to particles and their antiparticles.
- Note the significant discrepancy between the two Tevatron measurements (last two high energy points on the left panel in Fig. 5).
- Note also that the Pomeron's coupling to the pion is about 2/3 that to the nucleon (quark counting rule).

It is remarkable that such a simple fit works well all the way from such low energy to very high energies. At the lower-energy end of the plots, very little can be produced in the final state, just a very few pions. But as the energy increases, we cross thresholds for the production of charm, jets and much else. The total cross-section, however, is completely smooth and seems to be unaware of these thresholds.

When Donnachie and I first made these fits to total cross-section, the higher-energy data from the CERN collider and the Tevatron were not available, but our predictions based on Regge theory were successful.

The magnitude of the Pomeron's contribution to the Kp cross-section shown in Fig. 6 is a little less than to the πp: the coupling of the Pomeron to a strange quark is about 70% of that to the light quarks. The Pomeron's coupling to the pn and $\bar{p}n$ amplitudes (see again Fig. 6) is the same as to pp and $\bar{p}p$: it has the quantum numbers of the vacuum (like the f_2).

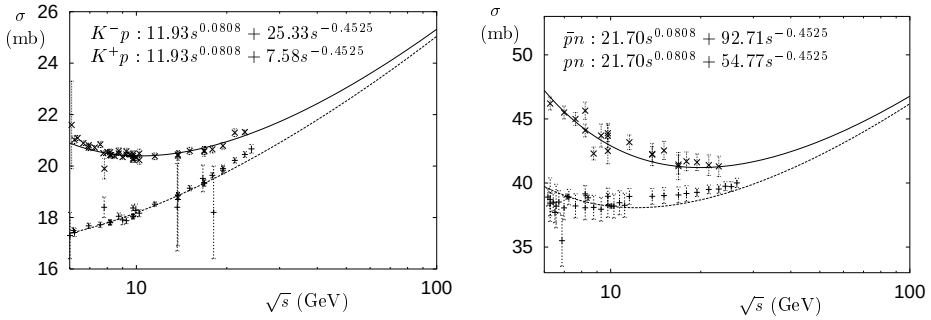

Fig. 6. Fits to total cross-sections for $K^{\pm}p$, pn and $\overline{p}n$ scattering.

Before the HERA measurements of the γp total cross-section, predictions for its value differed very widely. But the prediction from Regge theory depicted in Fig. 7 proved to be successful.

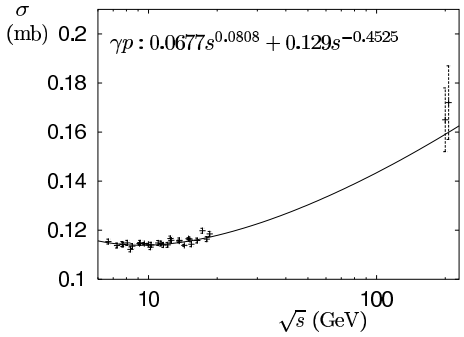

Fig. 7. Fit to total cross-section for γp scattering.

It is, however, well known that the power-like behaviour of the total cross-sections is incompatible with the Froissart–Łukaszuk–Martin bound which says that at very large s

$$\sigma^{\mathrm{TOT}}(s) < \frac{\pi}{m_\pi^2}\ \log^2\left(\frac{s}{s_0}\right) \tag{3}$$

for some unknown s_0 — probably of the order of 1 GeV^2. At LHC energy, this gives $\sigma^{\rm TOT} < 4.3$ barns. So the bound has little to do with physics!

Note that the proof depends on the partial-wave unitarity equation:

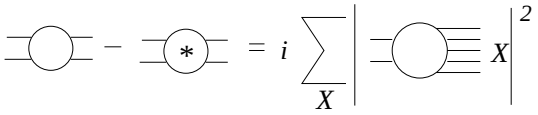

$$\text{Im } a_\ell(s) = |a_\ell(s)|^2 \ + \ \text{inelastic terms}$$

so that

$$|a_\ell(s)| < 1\,.$$

Therefore the bound applies only to hadron–hadron scattering.

Nevertheless, there is a wide belief that it applies also to photon and lepton-induced processes. To derive the bound for these processes, one has to use models or physical intuition. But it is far from certain that this is reliable under the extreme conditions that will operate at very high energies.

In principle, the photoproduction cross-section might become very large at high energy, and $F_2(x, Q^2)$ might become very large at small x.

A more stringent constraint follows from an obvious inequality:

$$\sigma^{\rm ELASTIC} < \sigma^{\rm TOTAL}\,.$$

In fact, unitarity can be used to show that even

$$\sigma^{\rm ELASTIC} < \tfrac{1}{2}\,\sigma^{\rm TOTAL}\,. \tag{4}$$

This is the *Pumplin Bound*.

Because Pomeron exchange alone gives

$$\sigma^{\rm TOTAL} \sim s^\epsilon\,, \qquad \epsilon \ \approx \ 0.08\,,$$

and

$$\left.\frac{d\sigma}{dt}^{\rm ELASTIC}\right|_{t=0} \ \sim \ s^{2\epsilon}$$

it violates the bound (4) at large s.

3. t dependence of high energy processes

Let us consider elastic scattering and assume that the Pomeron trajectory is linear (like ρ, ω, f_2, a_2):

$$\alpha_{I\!P}(t) = \epsilon_{I\!P} + \alpha'_{I\!P} t\,. \tag{5}$$

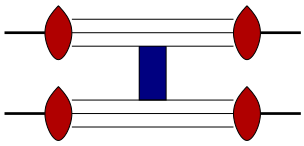

Fig. 8. Pomeron coupling to the separate quarks in a hadron.

As I pointed out in Section 2, total cross-section data suggest the quark counting rule: the Pomeron seems to couple to the separate quarks in a hadron with a γ^μ coupling (as expected if Pomeron exchange is two-gluon exchange):

$$A^{qq}_{I\!P}(s,t) \sim \bar\beta_{I\!P}(t)(\bar u_3\gamma^\mu u_1)(\bar u_4\gamma_\mu u_2)e^{-\frac{1}{2}i\pi\alpha_{I\!P}(t)}(\alpha'_{I\!P}s)^{\alpha_{I\!P}(t)-1}\,. \qquad (6)$$

The two-gluon-exchange model would make $\bar\beta_{I\!P}(t)$ essentially constant: $\bar\beta_{I\!P}(t) = \beta^2_{I\!P}$. For coupling to nucleons, we need isosinglet (sum of proton and neutron) $C = +$ Dirac and Pauli form factors $F_1(t)$ and $F_2(t)$. Assume they are the same as for $C = -$ photon exchange (this is unlikely to be quite right!). Then $F_2(t)$ is very small (at $t = 0$ it is the sum of the anomalous magnetic moments of the proton and neutron, 1.79–1.9). This means Pomeron exchange does not flip the nucleon helicity, which is found to be true. So

$$\frac{d\sigma}{dt} = \frac{[3\beta_{I\!P}F_1(t)]^4}{4\pi}(\alpha'_{I\!P}s)^{2(\epsilon_{I\!P}+\alpha'_{I\!P}t)}\,, \qquad (7)$$

where $\beta_{I\!P}$ and $\epsilon_{I\!P}$ are known from $\sigma^{\rm TOT}$. Therefore the only free parameter is $\alpha'_{I\!P}$. One can fix α' from the very-low-t data at some energy, say $\sqrt{s}$ =53 GeV shown in Fig. 9. This gives $\alpha' = 0.25$ GeV^{-2}.

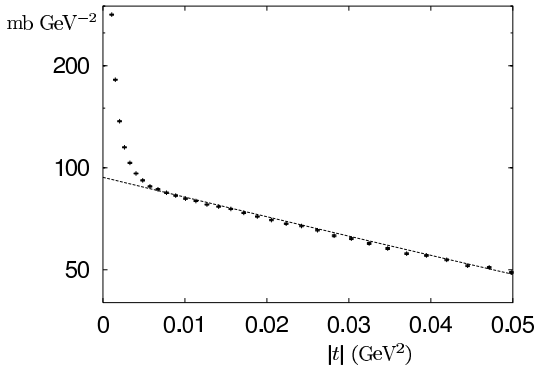

Fig. 9. $d\sigma/dt$ for small t.

Then the formula (7) works well out to larger t at the same energy, as it is shown in Fig. 10. It also fits well to pp and $p\bar{p}$ elastic scattering data at all other available energies. Because $F_1(t)$ is raised to the power 4 in the formula, this gives a good test that it is the correct form factor, but why this should be so is not understood.

Note that the curves do not include photon exchange, which contributes significantly at very small t.

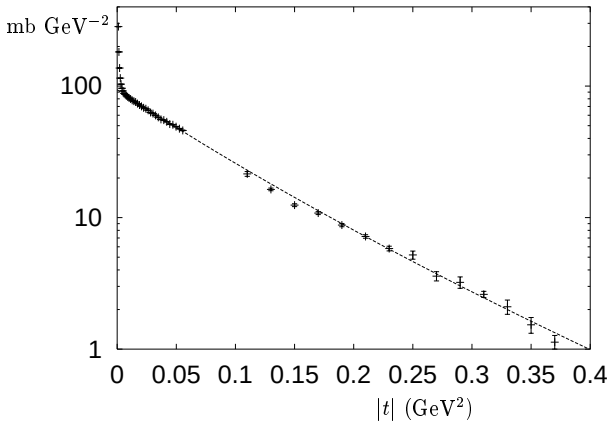

Fig. 10. $d\sigma/dt$ for larger range of t.

Because formula (7) contains the factor $\exp(2\alpha' t \log(\alpha' s))$, the contribution of Pomeron exchange to the forward peak in $d\sigma/dt$ becomes steeper as the energy increases. This is shown in Fig. 11.

Note again the discrepancy between the data from the two Tevatron experiments.

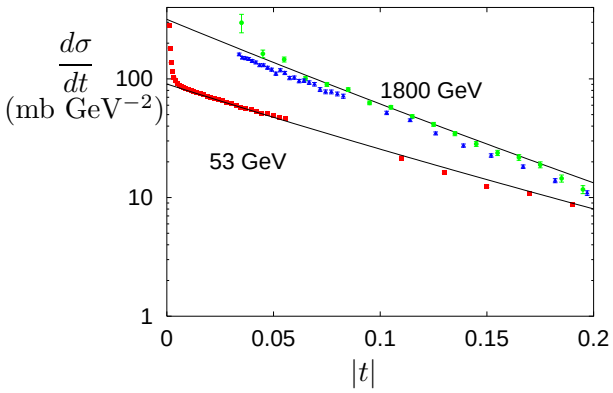

Fig. 11. Shrinkage of the forward peak.

We have now almost all ingredients to predict πp elastic scattering. The form factor $F_1(t)$ is raised to the power 4 in the pp-scattering formula because the Pomeron couples to each of the two protons, so that $[F_1(t)]^2$ appears in the amplitude, and one has to square the amplitude to get $d\sigma/dt$. $F_1(t)$ is multiplied by 3 because, according to the quark counting rule, the Pomeron couples to single quarks in the proton and there are three of them. If we want to extend the formula to πp scattering, we must replace $[3F_1(t)]^4$ with $[3F_1(t)]^2\ [2F_\pi(t)]^2$, where $F_\pi(t)$ is the elastic form factor of the pion. This has been measured and is shown in Fig. 12. We can plot now elastic cross-section for πp scattering (at $\sqrt{s} = 19.4$ GeV). The curve (shown in Fig. 13) has no free parameters!

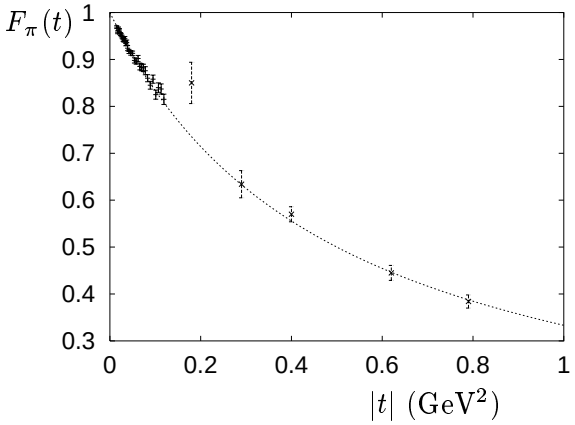

Fig. 12. Elastic form factor of the pion.

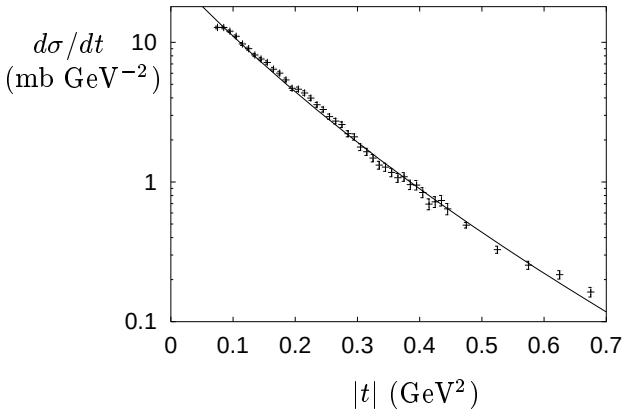

Fig. 13. Elastic cross-section for πp scattering (at $\sqrt{s} = 19.4$ GeV).

We can repeat analogous steps in the case of exclusive ρ photoproduction. To calculate the amplitude for $\gamma p \to \rho p$, we shall use vector dominance and assume the ρ behaves like the pion. The result is shown in Fig. 14. Again this calculation contains no free parameters! Note that both Pomeron exchange and vector-meson exchange are included in this calculation.

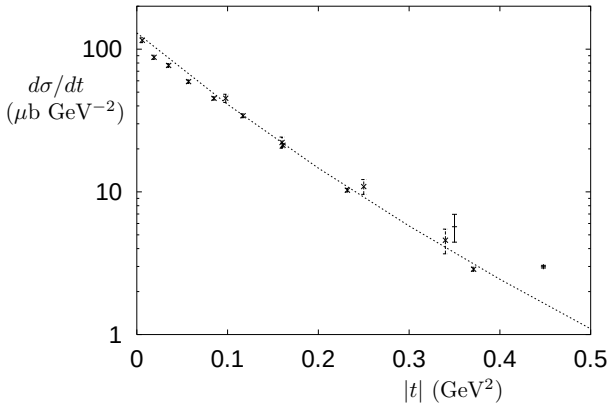

Fig. 14. Exclusive ρ photoproduction at $W = 71.7$ and 94 GeV from ZEUS.

Now we shall turn to pp elastic scattering at large t. For $|t|$ greater than about 3 Gev^2, the data are consistent with being energy-independent and fit well to a simple power of t:

$$\frac{d\sigma}{dt} = 0.09\, t^{-8}\,. \tag{8}$$

This behaviour, illustrated in Fig. 15, is what is calculated from triple-gluon exchange shown in Fig. 16.

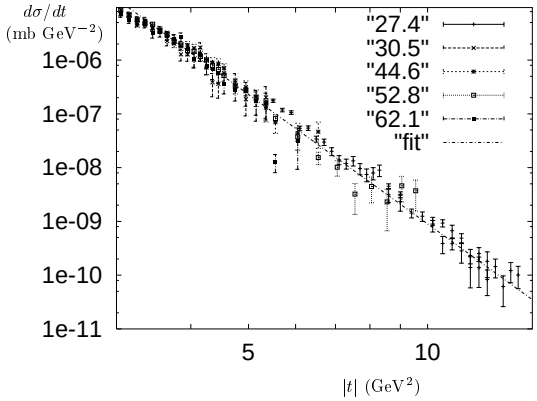

Fig. 15. pp elastic scattering at large t for different energies.

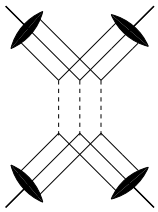

Fig. 16. Three gluon exchange in pp elastic scattering.

It is not understood why this simple mechanism, with no higher-order perturbative QCD corrections and fixed couplings α_S, should be what is needed. Note, though, that if the proton wave function is such that on average its momentum is shared equally among the three quarks, the momentum transfer carried by each gluon is only $t/9$ and so is quite small.

As I will explain, the data for $F_2(x, Q^2)$ suggest that there exists a second Pomeron, the hard Pomeron, with intercept $\alpha(0) \approx 1.4$. If we replace the gluons with this, we obtain a contribution that rises sharply with increasing energy. Although it is not seen in existing data, it might well become dominant at LHC energy, so that the large-t elastic scattering differential cross-section might be rather large.

Note that triple-gluon exchange is $C = -1$ – its contributions to the pp and $\bar{p}p$ amplitudes are opposite in sign.

At smaller values of t, the pp elastic scattering data show a striking dip structure shown in Fig. 17 (the 62 GeV data are multiplied by 10).

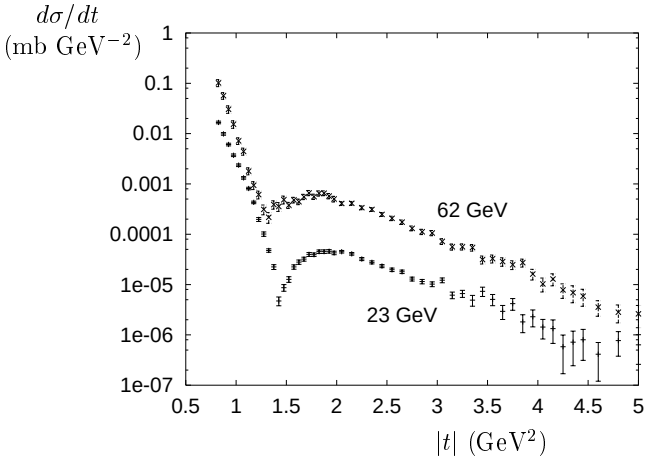

Fig. 17. Shrinking dip in pp elastic scattering.

It is not simple to construct an amplitude that reproduces these dips. The phase of the contribution from single-Pomeron exchange is given by the signature factor, so that at $-t \approx 1.4$ GeV^2 its real and imaginary parts are of similar magnitude. In order to cancel both of these at the same value of t, additional terms are needed. One of these is almost certainly the exchange of two Pomerons, but its phase is very different, so at least one other term is needed. Donnachie and I suggested that this is the triple-gluon-exchange contribution that is evident at larger values of t.

However, for $p\bar{p}$ scattering this has the opposite sign, which led us to predict that for this process the dip should be absent. This was confirmed in measurements at $\sqrt{s}$=53 GeV shown in Fig. 18.

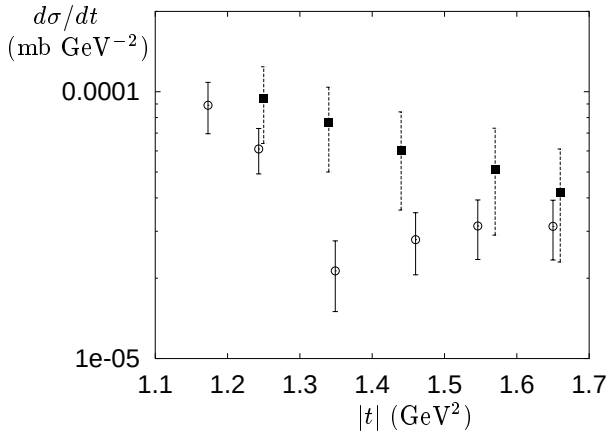

Fig. 18. $d\sigma/dt$, upper points for $\bar{p}p$, lower points for pp. No dip is seen for $\bar{p}p$ scattering.

A $C = -1$ exchange term such as triple-gluon exchange is known as an odderon exchange term. But there is no sign in the data of odderon exchange at $t = 0$.

4. Diffraction dissociation

This is the name given to the process

$$pp \to pX$$

depicted in Fig. 19, with the final proton loosing only a very small fraction ξ of its initial momentum (so therefore there is a large rapidity gap).

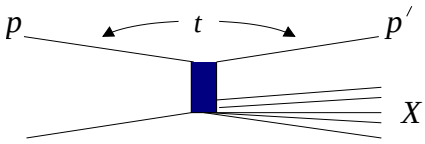

Fig. 19. Diffractive dissociation in pp scattering.

If we square the amplitude and sum over X we arrive at a diagram shown in Fig. 20. We need the imaginary part of the big lower bubble (compare the optical theorem). When its energy M_X is large we can apply Regge theory to it and so we get the triple-Regge diagram shown in Fig. 21.

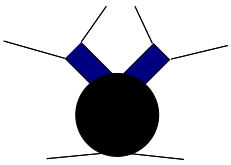

Fig. 20. Cross-section for the diffractive dissociation.

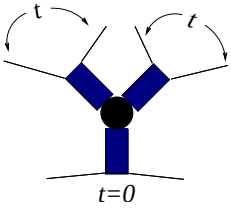

Fig. 21. Triple-Regge coupling.

It is not enough just to include the triple Pomeron! A very large number of terms need to be considered:

$$\begin{array}{cccccc} I\!P\,I\!P & I\!P\,I\!P & f_2 I\!P & I\!P\, f_2 & f_2 I\!P & \omega I\!P \\ I\!P & f_2 & I\!P & I\!P & f_2 & \omega \end{array} \quad \cdots$$

A term $\binom{12}{3}$ contributes to $d^2\sigma/dt\,d\xi$

$$f_1^a(t) f_2^a(t) f_3^b(0) G_3^{12}(t)\, e^{i(\phi(\alpha_1(t))-\phi(\alpha_2(t)))} \xi^{1-\alpha_1(t)-\alpha_2(t)} \left(\frac{M^2}{s_0}\right)^{\alpha_3(0)-1}, \quad (9)$$

with

$$\phi(\alpha(t)) = \begin{cases} -\frac{1}{2}\pi\alpha(t) & C=+1\,, \\ -\frac{1}{2}\pi(\alpha(t)-1) & C=-1\,. \end{cases} \quad (10)$$

Using a combination of terms, it is not difficult to get good fits to restricted sets of data. An example is shown in Fig. 22.

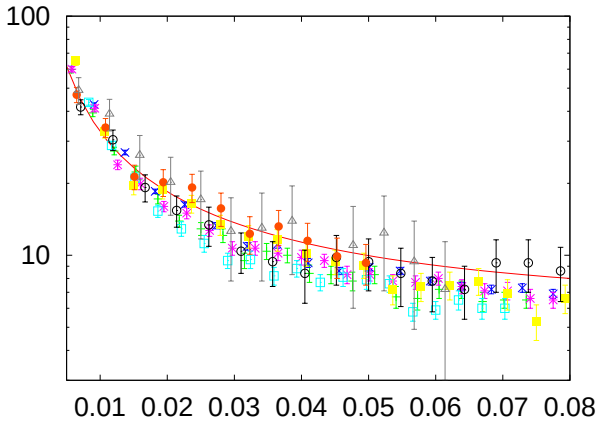

Fig. 22. Data at $-t = 0.25$ GeV^2 plotted against ξ from two experiments at the CERN ISR at $\sqrt{s}$ from 23 to 38 GeV, with a simple triple-Regge fit.

However, there are other data which are much more difficult to accommodate, for example the fixed-target data shown in Fig. 23.

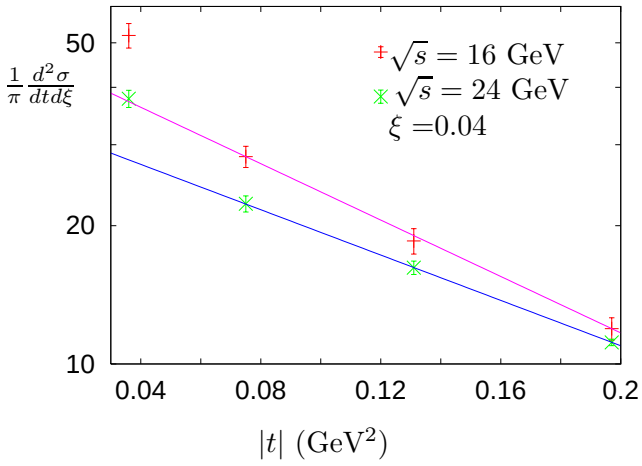

Fig. 23. Fixed target data.

Notice two characteristics of these data: the cross-section decreases as the energy increases, and while a simple exponential in t fits well to the three highest-t values at each energy, it fails to describe the lowest-t points.

All too often, fits are made to a restricted set of data using only Pomeron exchange, with the result that conclusions are reached that are almost certainly wrong.

The data at higher energies present severe problems. Sadly, the UA4 data for $d^2\sigma/dt\ d\xi$ have been lost. CDF publish no data points, just their fit. UA4 data for $d\sigma/dt$ survive, that is $d^2\sigma/dt\ d\xi$ integrated over a certain range of ξ. The result of integrating the CDF fit similarly is shown in Fig. 24. There is an obvious problem!

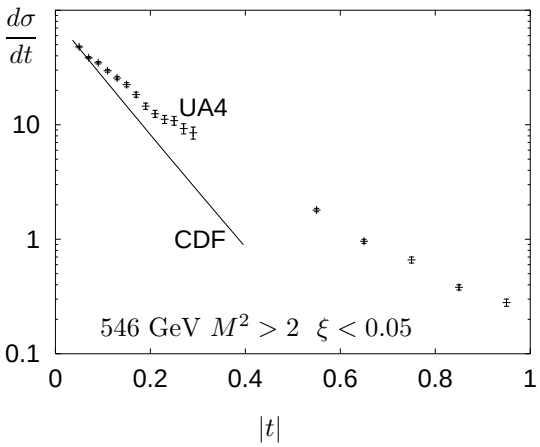

Fig. 24. UA4 data for $d\sigma/dt$ and the CDF fit.

5. Deep inelastic lepton scattering

In this section we shall apply Regge theory to deep inelastic lepton–proton scattering depicted in Fig. 25.

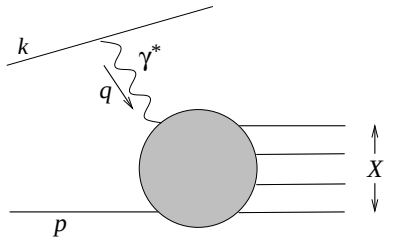

Fig. 25. Deep inelastic lepton–proton scattering.

Define

$$W^2 = (p+q)^2\,, \qquad \nu = pq\,, \qquad Q^2 = -q^2\,, \qquad x = Q^2/(2\nu)\,.$$

Soft-Pomeron exchange contributes a behaviour $(W^2)^{0.08}$ at fixed Q^2. I have shown how this describes the data well for $Q^2 = 0$. But the W dependence gets steeper as Q^2 increases, as shown in Fig. 26. At large Q^2 the behaviour is about $(W^2)^{0.4}$.

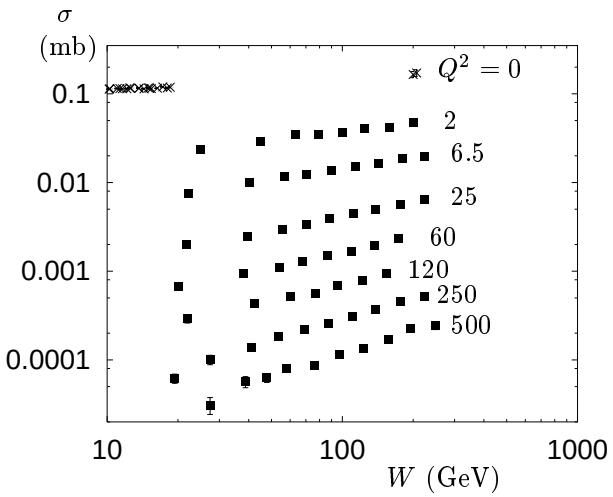

Fig. 26. DIS data for different Q^2.

The theory of the W dependence is not well understood. Define

$$\sigma\left(W^2, Q^2\right) = \frac{4\pi^2 \alpha_{\rm EM}^2}{Q^2} F_2\left(x, Q^2\right) . \tag{11}$$

Two alternative theoretical possibilities:

- A $(W^2)^{0.4}$ term is there at all Q^2, but at $Q^2 = 0$ its contribution is very small.
- It is not there at $Q^2 = 0$, but as Q^2 increases it is gradually generated through perturbative QCD evolution.

The second approach is conventional, but it has a mathematical problem, as I will shortly explain. The first leads to the possibility that $\sigma(pp)$ also has an $s^{0.4}$ term, so that the LHC total cross-section is big.

5.1. Simple Regge fit

We shall discuss now simple Regge fit to the DIS data. Soft Pomeron exchange contributes to $F_2(x, Q^2)$ at large W a term that behaves as $(W^2)^{\epsilon_1}$, with $\epsilon_1 \approx 0.08$. This is equivalent to $(1/x)^{\epsilon_1}$ at large $1/x$, say $1/x > 10^3$.

At smaller values of $1/x$, we must add in f_2 and a_2 exchange, and include a multiplicative factor in each term so as to make it go to 0 appropriately as $x \to 1$. To begin with let me restrict the discussion to $x < 10^{-3}$.

We have seen that soft-Pomeron exchange is not enough, so Donnachie and I added in another term which we call hard-Pomeron exchange. It behaves as $(1/x)^{\epsilon_0}$, and I have shown that we need $\epsilon_0 \approx 0.4$. In order to pin down the contribution from this term, we went through a number of steps:

1. Take

$$F_2\left(x, Q^2\right) = f_0\left(Q^2\right) x^{-\epsilon_0} + f_1\left(Q^2\right) x^{-\epsilon_1}\,, \qquad x < 10^{-3}\,.$$

In order to get information about the unknown functions $f_0(Q^2)$ and $f_1(Q^2)$, choose a value for ϵ_0 somewhat less than 0.4 and another somewhat greater. Then fit the available data at each Q^2. This gives the outputs for the two functions shown in Fig. 27.

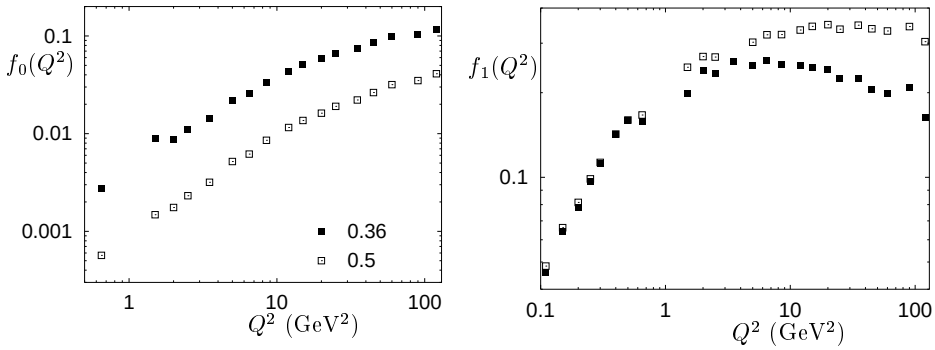

Fig. 27. Functions f_0 and f_1. The black points are for $\epsilon_0 = 0.36$, and the white points $\epsilon_0 = 0.5$.

In each case, $f_0(Q^2)$ rises steadily with Q^2, while $f_1(Q^2)$ either goes to a constant or rises to a peak and then slowly decreases.

2. This suggests parametrisations of $f_0(Q^2)$ and $f_1(Q^2)$. Current conservation implies that near $Q^2 = 0$ at fixed W, $F_2(x, Q^2)$ vanishes like Q^2. Therefore $f_i(Q^2) \sim (Q^2)^{1+\epsilon_i}$. Take

$$\begin{aligned} f_0\left(Q^2\right) &= A_0 \left(\frac{Q^2}{1+Q^2/Q_0^2}\right)^{1+\epsilon_0} \left(1+Q^2/Q_0^2\right)^{\epsilon_0/2}\,, \\ f_1\left(Q^2\right) &= A_1 \left(\frac{Q^2}{1+Q^2/Q_1^2}\right)^{1+\epsilon_1}\,. \end{aligned}$$

For simplicity, this choice makes $f_1(Q^2)$ go to a constant at large Q^2. Although its contribution for $x < 0.001$ is fairly small, we include also an f_2, a_2 exchange term, that is we add

$$f_R\left(Q^2\right) x^{-\epsilon_R}\,, \qquad \epsilon_R = -0.4525$$

and use a similar parametrisation for $f_2(Q^2)$ to that for $f_1(Q^2)$:

$$f_R\left(Q^2\right) = A_R \left(\frac{Q^2}{1+Q^2/Q_R^2}\right)^{1+\epsilon_R}\,.$$

3. Now go back and again fit the data for $x < 0.001$, this time with ϵ_0 as one of the free parameters. Include also the photoproduction data and restrict to $W > 6$ GeV. This gives

$$\epsilon_0 = 0.41\,, \quad Q_0 = 2.9 \text{ GeV}\,, \quad Q_1 = 770 \text{ MeV}\,, \quad Q_R = 465 \text{ MeV}\,,$$

$$A_0 = 0.0022\,, \quad A_1 = 0.60\,, \quad A_R = 1.2$$

with $\chi^2 = 0.95$ per data point (190 data points), see Fig. 28. (The values of A_1, A_2 are determined largely by the real-photon data.)

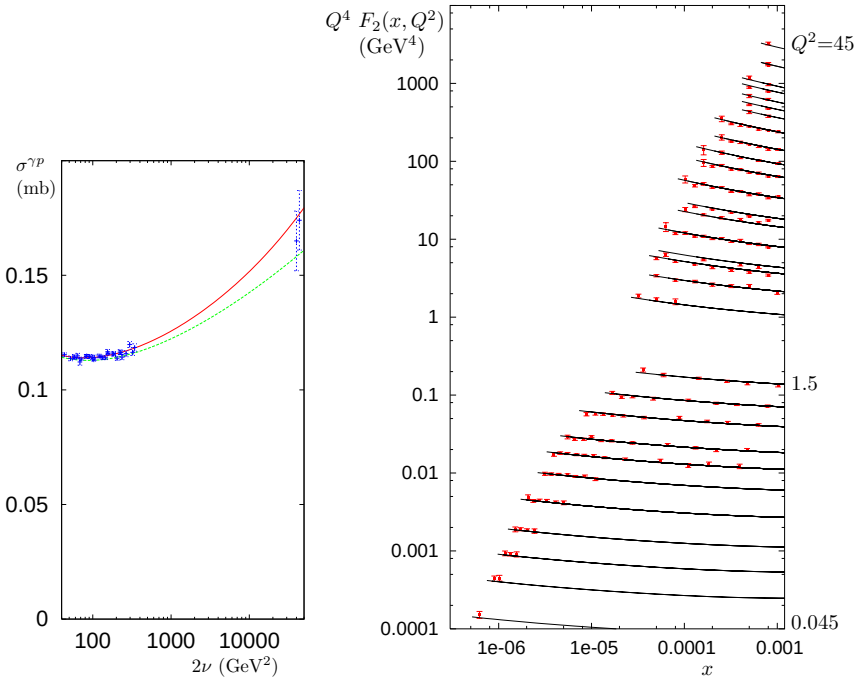

Fig. 28. Regge fit to small x DIS data.

Parametrisations in which $f_0(Q^2)$ falls slowly at large Q^2, for example like $1/Q$, also describe the data well. If only for this reason, the error on the determination of ϵ_0 is quite large, say $\epsilon_0 = 0.41 \pm 0.06$.

4. There are data at larger Q^2 but at larger x. Introduce powers of $(1-x)$ in each term given by the dimensional counting rule. This is not correct, but better than nothing, and using the values of the parameters that have already been determined by the data for $x < 0.001$ they give surprisingly good fits out to very large Q^2, see Fig. 29.

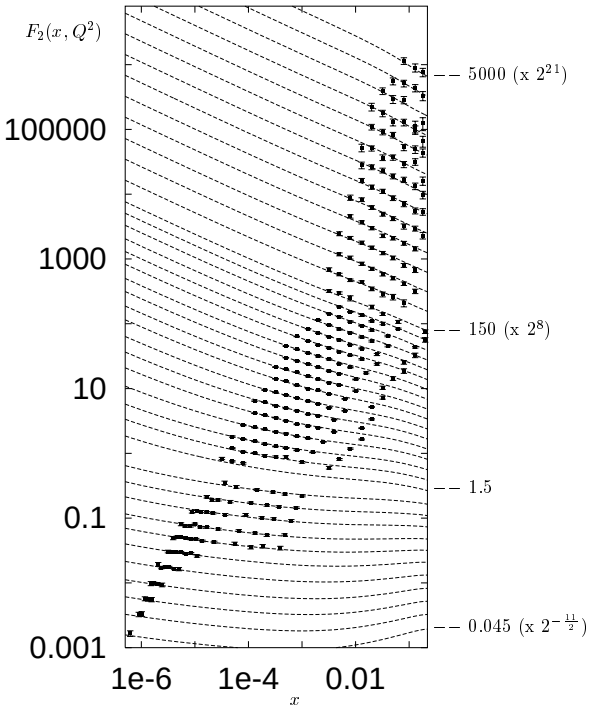

Fig. 29. Regge fit to larger x DIS data.

5.2. Charm

The data for the charm contribution $F_2^c(x,Q^2)$ display a very interesting simplicity. Even at small Q^2, they agree well with a fixed power of $1/x$ close to 0.4 as can be seen from Fig. 30. The lines are just $2/5$ of the hard-Pomeron contribution to the complete $F_2(x,Q^2)$. The factor $2/5$ suggests that the coupling of the hard Pomeron to the c quark has the same strength as to the light quarks. The data do not allow more than an extremely small contribution from soft-Pomeron exchange.

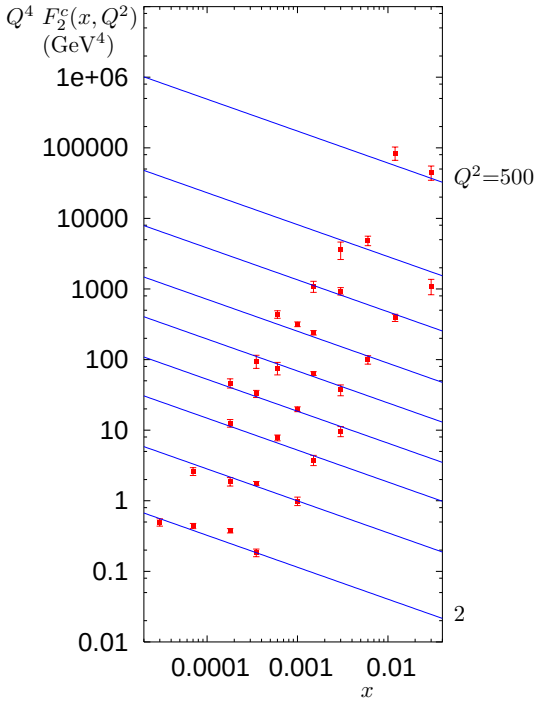

Fig. 30. $Q^2\,F_2^c(x,Q^2)$ as function of x for $Q^2 = 500$ GeV^2.

So only the hard Pomeron couples to charm, a result that I find surprising. It seems to be true even at $Q^2 = 0$ as shown in Fig. 31.

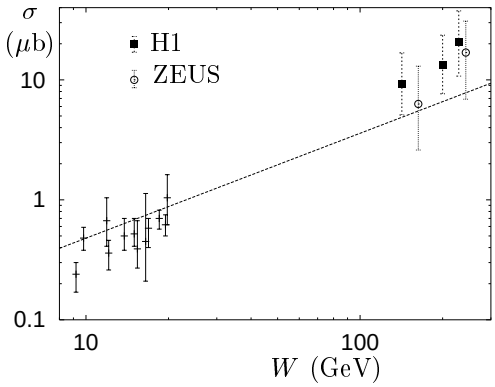

Fig. 31. Charm photoproduction cross-section in DIS.

6. Perturbative QCD and Regge theory

Perturbative QCD and Regge theory have to live together. To see how it happens consider the singlet DGLAP equation is:

$$\frac{\partial}{\partial t}\boldsymbol{u}\left(x,Q^2\right) = \int_x^1 dz\,\boldsymbol{P}\left(z,\alpha_{\rm s}\left(Q^2\right)\right)\,\boldsymbol{u}\left(x/z,Q^2\right)\,,$$
$$\boldsymbol{u}\left(x,Q^2\right) = \begin{pmatrix} q\left(x,Q^2\right) \\ g\left(x,Q^2\right)\end{pmatrix}. \tag{12}$$

It simplifies if we Mellin transform with respect to x. That is, define

$$\boldsymbol{u}\left(N,Q^2\right) = \int_0^1 dx\,x^{N-1}\boldsymbol{u}\left(x,Q^2\right)\,, \tag{13}$$

$$\boldsymbol{P}\left(N,\alpha_{\rm s}\left(Q^2\right)\right) = \int_0^1 dz\,z^N\boldsymbol{P}\left(z,\alpha_{\rm s}\left(Q^2\right)\right)\,. \tag{14}$$

Then

$$\frac{\partial}{\partial t}\boldsymbol{u}\left(N,Q^2\right) = \boldsymbol{P}\left(N,\alpha_{\rm s}\left(Q^2\right)\right)\,\boldsymbol{u}\left(N,Q^2\right). \tag{15}$$

If $\boldsymbol{u}(x,Q^2)\sim\boldsymbol{f}(Q^2)x^{-\epsilon}$ at small x, then $\boldsymbol{u}(N,Q^2)$ has a pole

$$\frac{\boldsymbol{f}\left(Q^2\right)}{N-\epsilon}\,. \tag{16}$$

Insert this in the DGLAP equation. The pole singularities on the two sides of the equation must balance as $N\to\epsilon_0$:

$$\frac{\partial}{\partial t}\boldsymbol{f}\left(Q^2\right) = \boldsymbol{P}\left(N=\epsilon,\alpha_{\rm s}\left(Q^2\right)\right)\,\boldsymbol{f}\left(Q^2\right)\,. \tag{17}$$

For hard-Pomeron exchange, with $\epsilon\approx 0.4$, expand the matrix $\boldsymbol{P}(\epsilon,\alpha_{\rm s})$ in powers of $\alpha_{\rm s}$. This is not valid for soft-Pomeron exchange, $\epsilon\approx 0.08$, because the elements of $\boldsymbol{P}$ are singular at $N=0$.

This is a problem with all applications of pQCD to the evolution of $F_2(x,Q^2)$, though usually it is a problem that is hidden.

To solve the differential equation, we need initial conditions at some Q^2, *e.g.* at $Q^2=20$ GeV^2. We saw that for $F_2^c(x,Q^2)$ soft-Pomeron exchange is extremely small. So pQCD suggests that this is true also for $g(x,Q^2)$.

The upper curves in Fig. 32 come from the fit to the data that I have described. The lower curves are the solution to the DGLAP equation, using values of $\Lambda_{\rm QCD}$ similar to what are usually accepted:

$$\Lambda^{\rm LO} = 140 \text{ MeV}\,, \qquad \Lambda^{\rm NLO} = 330 \text{ MeV}\,.$$

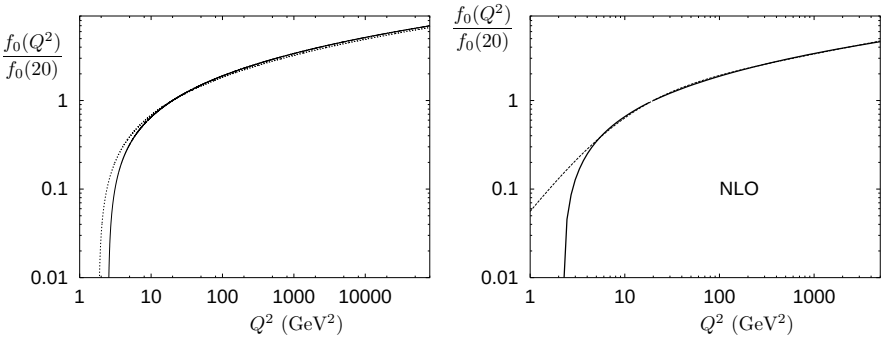

Fig. 32. QCD evolution of f_0 at leading order (left) and next to leading order (right).

Note that the DGLAP equation is supposed to be valid only for large Q^2; evidently this means Q^2 greater than about 5 GeV^2. It is interesting that the LO and NLO results are not very different.

It is interesting also that the upper curves behave as a power of Q^2 at large Q^2, because that is how we chose to parametrise $f_0(Q^2)$. But the outputs from the DGLAP calculations rather behave as power of $\log(Q^2)$. Numerically, they are almost identical over a very large range of Q^2 values.

Because the gluon density is dominated at all Q^2 by hard Pomeron exchange alone, that is it behaves approximately as $x^{-0.4}$ for all Q^2, it is rather larger (DL) than is conventionally supposed (MRST or CTEQ), particularly at small Q^2. This is shown in Fig. 33.

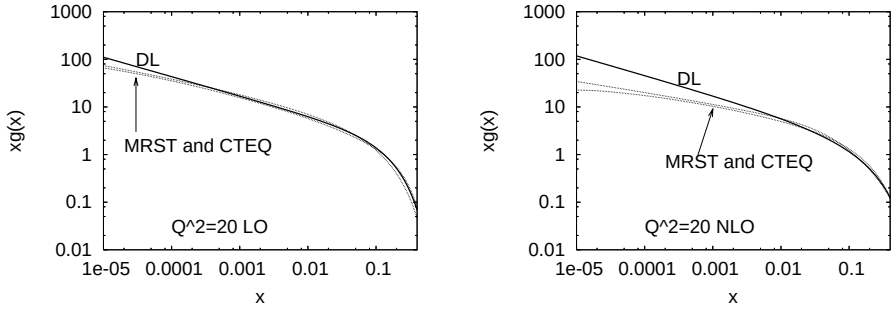

Fig. 33. Gluon distribution at leading order (left) and next to leading order (right).

7. Regge theory for other high energy processes

7.1. Photon–photon scattering

It is interesting to test Regge factorisation in photon–photon scattering. For each of the separate exchanges hard Pomeron, soft Pomeron and Reggeon the following relation holds:

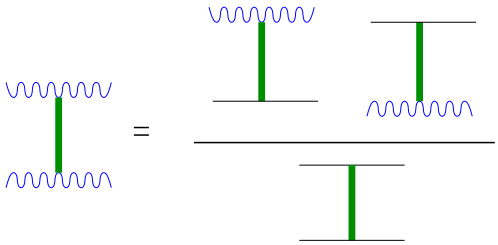

This is valid if the exchange corresponds to a pole in the complex-ℓ plane, because for each exchange the contribution is the product of a coupling at each vertex and a "propagator" corresponding to the other factors in the Regge formula, including the power of s. Thus, for each term, the contribution satisfies

$$\sigma(\gamma\gamma) = \frac{\sigma(\gamma p)\sigma(\gamma p)}{\sigma(pp)} \quad \text{for all} \quad Q_1^2, Q_2^2\,.$$

For $\gamma\gamma$ we must add in the box graph (see Fig. 34) summed over the possible quark flavours in the loop. It is particularly important when the energy is not very large.

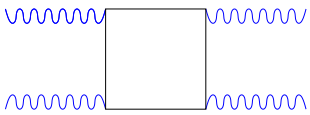

Fig. 34. Perturbative contribution to γ–γ scattering.

In the case of real photons, the fits I have described for $\sigma(\gamma p)$ and $\sigma(pp)$ yield the result for $\sigma(\gamma\gamma)$ that is shown in Fig. 35. The experimental data are uncertain because of the need to make large acceptance corrections, and different models for calculating these lead to rather different outputs, as is seen in the plot.

We may similarly calculate the charm component of $\sigma(\gamma\gamma)$ as shown in Fig. 36.

In each case, the blue (lower) curves are the hard-Pomeron contribution. The box graph is what causes the cross-section initially to fall with increasing W.

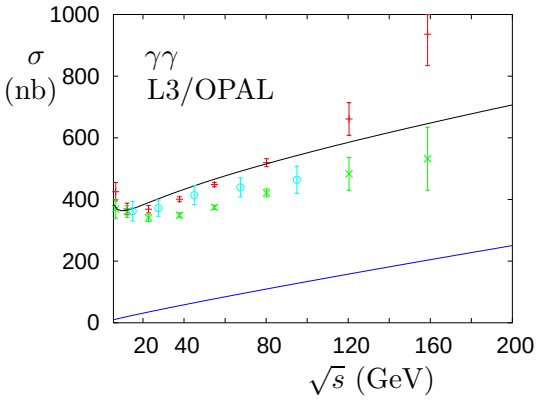

Fig. 35. Cross-section for γ–γ scattering.

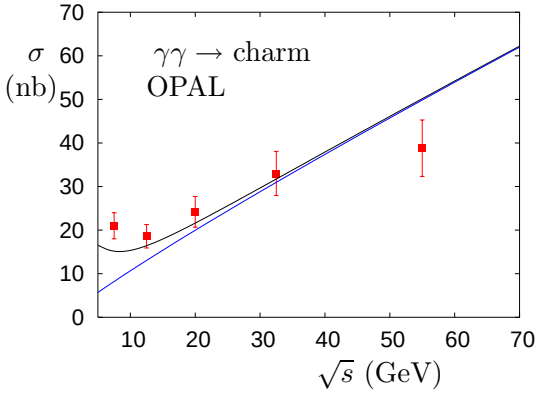

Fig. 36. Cross-section for charm production in γ–γ scattering.

When one photon is on shell and the other off shell, a similar calculation gives the photon structure function shown in Fig. 37.

When both photons are off shell we get the cross-section shown in Fig. 38. In each case, the blue (lower) curves are the hard-Pomeron contribution.

At this point it is difficult to draw any conclusion about Regge factorisation: the data are not good enough.

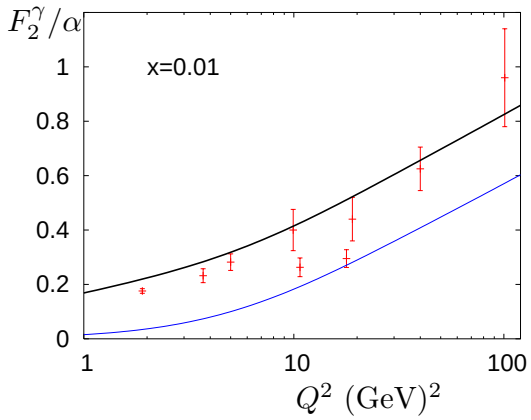

Fig. 37. Photon structure function.

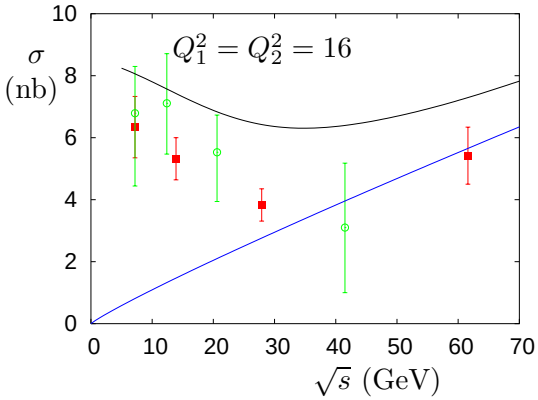

Fig. 38. Cross-section for $\gamma^* - \gamma^*$ scattering.

7.2. $\gamma p \to J/\psi\ p$

Parametrise the amplitude as a sum of hard Pomeron + soft Pomeron + Reggeon exchange and adjust the relative contributions so as to fit the data for $d\sigma/dt$. Because the Regge signature factor gives each term a different phase, the resulting amplitude is not altogether simple. The result is shown in Fig. 39.

The fit needs the hard Pomeron slope to be quite small, perhaps 0.05. Integrating over t, we find the result shown in Fig. 40.

The blue (lower) line is from the hard-Pomeron term alone. Why does the soft Pomeron couple to $\gamma p \to J/\psi\, p$ but not to F_2^c? The explanation may be found in data from the Omega experiment [2]:

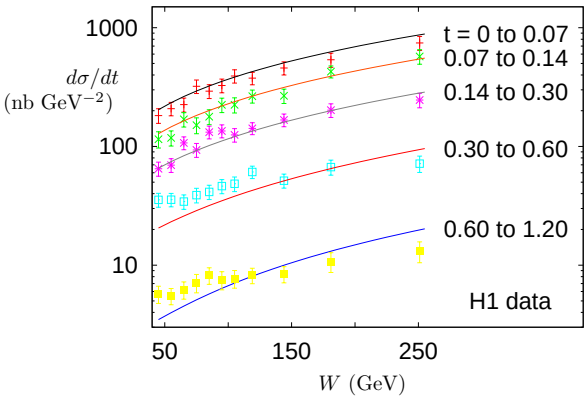

Fig. 39. Cross-section for $\gamma p \to J/\psi\ p$.

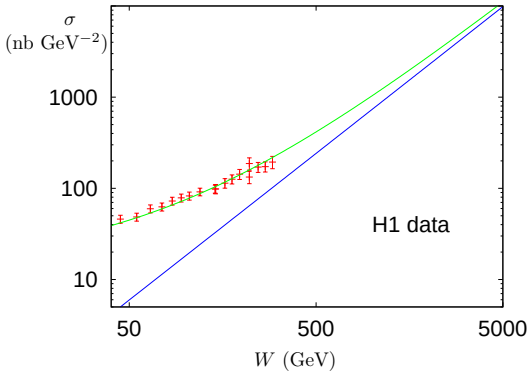

Fig. 40. Integrated cross-section for $\gamma p \to J/\psi\ p$ as a function of W.

$$\frac{\bar{p}\,\mathrm{Cu} \to J/\psi\, X}{p\,\mathrm{Cu} \to J/\psi\, X} \approx 6\,.$$

So the valence quarks of the beam couple to J/ψ: $|c\bar{c}\rangle$ mixes with $|q\bar{q}>$ and the J/ψ is not pure $c\bar{c}$.

7.3. Hard Pomeron in hadron–hadron scattering?

Given that the hard Pomeron exists, does it contribute to pp and $p\bar{p}$ scattering? Try including its contribution in the fits to the total cross-section. That is, use hard Pomeron, soft Pomeron and Reggeon exchange:

$$\begin{aligned} &\sigma(pp), \sigma(p\bar{p}), \sigma(\gamma p): && \sigma = X_0 s^{\epsilon_0} + X_1 s^{\epsilon_1} + X_R s^{\epsilon_R}\,, \\ &F_2\left(x, Q^2\right): && x^{-\epsilon_0} f_0\left(Q^2\right) + x^{-\epsilon_1} f_1\left(Q^2\right) + x^{-\epsilon_R} f_R\left(Q^2\right)\,. \end{aligned}$$

The resulting fits, with

$$\epsilon_0 = 0.45\,, \qquad \epsilon_1 = 0.067\,, \qquad \epsilon_R = -0.48\,,$$

are shown in Fig. 41. The lower (blue) lines are the hard Pomeron contribution.

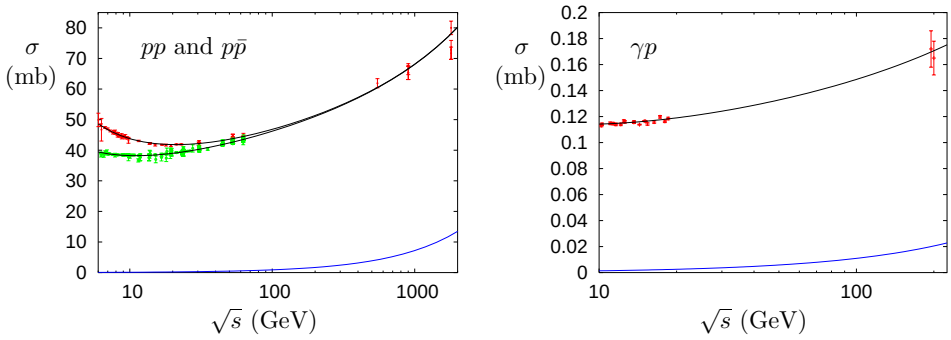

Fig. 41. Regge fits with hard Pomeron contribution (lower curves).

We can extrapolate these fits to the LHC energies. This is shown in Fig. 42.

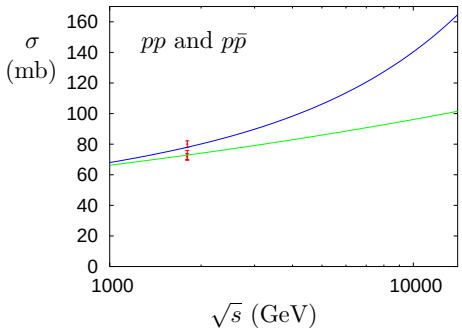

Fig. 42. Regge fits extrapolated to the LHC energies. The lower line is the original fit with a hard Pomeron contribution.

At these energies we have to worry about unitarity, however, we do not know how to do that. We need to sum single-$I\!P$, double-$I\!P$, ... exchanges:

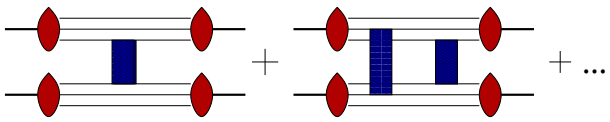

Although we know some general properties of these additional terms, we cannot calculate them. The double-$I\!P$-exchange term has the general structure

$$A_{I\!P_1 I\!P_2}(s,t) \sim \beta(t)\ s^{\alpha_{I\!P_1 I\!P_2}(t)}(\log(s))^{-\gamma(t)}\,. \tag{18}$$

For linear trajectories,

$$\begin{aligned} \alpha_{I\!P_1 I\!P_2}(t) &= \alpha_{I\!P_1 I\!P_2}(0) + \alpha'_{I\!P_1 I\!P_2} t\,, \\ \alpha_{I\!P_1 I\!P_2}(0) &= \alpha_{I\!P_1(0)} + \alpha_{I\!P_2}(0) - 1\,, \\ \alpha'_{I\!P_1 I\!P_2} &= \frac{\alpha'_{I\!P_1}\alpha'_{I\!P_2}}{\alpha'_{I\!P_1} + \alpha'_{I\!P_2}}\,. \end{aligned} \tag{19}$$

But $\beta(t)$ and $\gamma(t)$ are unknown. Evidently, $\beta(t)$ depends on information about two-quark correlations in the proton wave function.

8. Eikonal model for *pp* scattering

This model has no theoretical foundation, but it produces multiple-exchange terms of the correct general structure.

In the CM frame

$$\begin{aligned} p_1 &= \left(E, \boldsymbol{p} + \tfrac{1}{2}\boldsymbol{q}\right)\,, \qquad p_3 = \left(E, \boldsymbol{p} - \tfrac{1}{2}\boldsymbol{q}\right)\,, \\ p_2 &= \left(E, -\boldsymbol{p} - \tfrac{1}{2}\boldsymbol{q}\right)\,, \qquad p_4 = \left(E, -\boldsymbol{p} + \tfrac{1}{2}\boldsymbol{q}\right) \end{aligned} \tag{20}$$

with $(\boldsymbol{p} + \frac{1}{2}\boldsymbol{q})^2 = (\boldsymbol{p} - \frac{1}{2}\boldsymbol{q})^2$ so that $\boldsymbol{p}.\boldsymbol{q} = 0$ and therefore $\boldsymbol{q}$ is in the two-dimensional space perpendicular to $\boldsymbol{p}$. Also $t = -\boldsymbol{q}^2$.

Write the amplitude as a 2-dimensional Fourier integral

$$\begin{aligned} A\left(s, -\boldsymbol{q}^2\right) &= 4\int d^2b\, e^{-i\boldsymbol{q}.\boldsymbol{b}} \tilde{A}\left(s, \boldsymbol{b}^2\right)\,, \\ \tilde{A}\left(s, \boldsymbol{b}^2\right) &= \frac{1}{16\pi^2}\int d^2q\, e^{i\boldsymbol{q}.\boldsymbol{b}} A\left(s, -\boldsymbol{q}^2\right) \end{aligned} \tag{21}$$

$\boldsymbol{b}$ is called the impact parameter.

Define

$$\chi(s,b) = -\log\left(1 + 2i\tilde{A}/s\right)$$

so that

$$\tilde{A}\left(s, \boldsymbol{b}^2\right) = \tfrac{1}{2} is\left(1 - e^{-\chi(s,b)}\right)\,.$$

Remember the unitarity condition

$$\text{Im}\ a_\ell(s) = |a_\ell(s)|^2\ +\ \text{inelastic terms}$$

so that $|a_\ell(s)| < 1\,.$

One can show that this is satisfied if

$$\text{Re}\ \chi(s,b) \geq 0\,.$$

Expand the exponential as a power series:

$$\begin{aligned} A\left(s,-\boldsymbol{q}^2\right) &= 2is\int d^2b\, e^{-i\boldsymbol{q}.\boldsymbol{b}}\left(1-e^{-\chi(s,b)}\right) \\ &= 2is\int d^2b\, e^{-i\boldsymbol{q}.\boldsymbol{b}}\left(\chi-\frac{\chi^2}{2!}+\frac{\chi^3}{3!}\ldots-\frac{(-\chi)^n}{n!}\ldots\right)\,. \end{aligned} \quad (22)$$

If first term is approximated by single-$I\!P$ exchange, the second has the correct general structure of double-$I\!P$ exchange, *etc.* And one can show that then at very large s

$$\sigma^{\text{TOT}} \sim 4\pi\alpha'\epsilon_0(\log s)^2 \quad (23)$$

so the Froissart bound is satisfied.

But, although it has been widely used, this representation for the amplitude has little theoretical foundation. For example, the double-exchange term should contain information about the two-quark correlation in the proton's wave function, but this is not present in the term χ^2.

Let us now apply the eikonal model to pp elastic scattering. The fit to $d\sigma/dt$ using just the two single Pomeron exchanges and Reggeon exchange agrees well with the data at small t, but not at larger t as shown in Fig. 43.

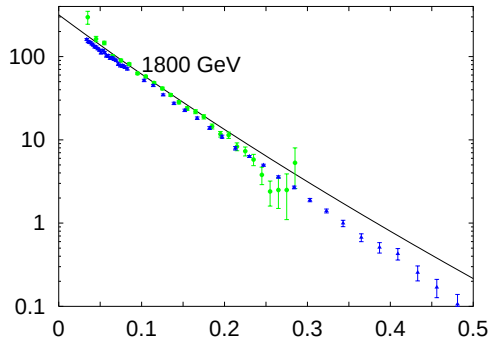

Fig. 43. $d\sigma/dt$ for pp scattering in the eikonal model.

From its general structure, we know that $I\!P I\!P$ exchange pulls $d\sigma/dt$ down at larger t. But nobody knows how to calculate it!

As a simple model, calculate $\chi(s,b)$ as the sum of the three single exchanges and take

$$\tilde{A}(s,b) = 2is\Big(\chi(s,b) - \lambda[\chi(s,b)]^2\Big)$$

together with a triple-gluon exchange term. Then repeat the fit, choosing λ to get pp dips at the right t as shown in Fig. 44.

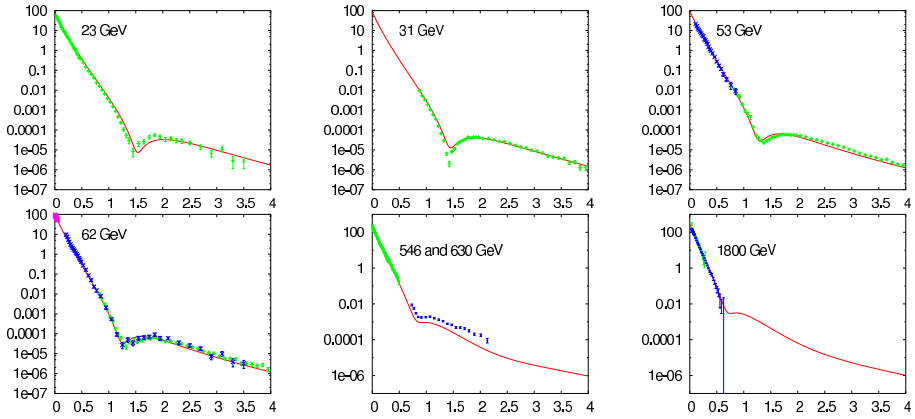

Fig. 44. Fitting dips in the eikonal model.

9. Conclusion

We conclude by showing the extrapolation to the LHC energy that is given now by the upper curve in Fig. 45. The lower curve is the fit with no hard-Pomeron contribution.

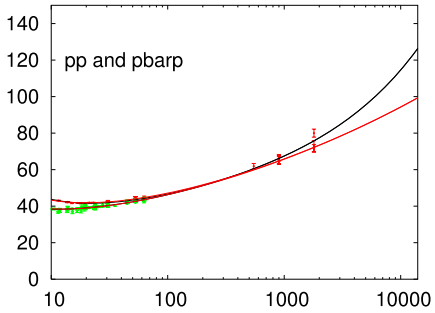

Fig. 45. Extrapolation of the total cross-sections to the LHC energies.

This procedure is highly model-dependent, so the error is inevitably large:

$$\sigma(\mathrm{LHC}) = 125 \pm 25 \text{ mb}\,. \tag{24}$$

REFERENCES

[1] S. Donnachie, G. Dosch, P. Landshoff, O. Nachtmann, *Pomeron Physics and QCD*, Cambridge Monographs on Particle Physics, Nuclear Physics, and Cosmology, Vol. 19, Cambridge University Press, 2002.

[2] M.J. Corden *et al.*, *Phys. Lett.* **68B**, 96 (1977).